High friction on a bubble mattress

AUDREY STEINBERGER[1,2], CÉCILE COTTIN-BIZONNE[1,2]*, PASCAL KLEIMANN[2,3] AND ELISABETH CHARLAIX[1,2]

[1]Université de Lyon, CNRS UMR 5586, Laboratoire PMCN, F-69622 Villeurbanne, France
[2]Université Lyon 1, Lyon, F-69622, France
[3]Institut des Nanotechnologies de Lyon, INL, Université de Lyon, Lyon, F-69003, France
*e-mail: ccottin@lpmcn.univ-lyon1.fr

Published online: 22 July 2007; doi:10.1038/nmat1962

Reducing the friction of liquid flows on solid surfaces has become an important issue with the development of microfluidics systems, and more generally for the manipulation of fluids at small scales. To achieve high slippage of liquids at walls, the use of gas as a lubricant[1–4]—such as microbubbles trapped in superhydrophobic surfaces[5]—has been suggested. The effect of microbubbles on the effective boundary condition has been investigated in a number of theoretical studies[6–9], which basically show that on flat composite interfaces the magnitude of the slippage is proportional to the periodicity of the gaseous patterns[10]. Recent experiments aiming to probe the effective boundary condition on superhydrophobic surfaces with trapped bubbles have indeed shown high slippage in agreement with these theoretical predictions[10–12]. Here, we report nanorheology measurements of the boundary flow on a surface with calibrated microbubbles. We show that gas trapped at a solid surface can also act as an anti-lubricant and promote high friction. The liquid–gas menisci have a dramatic influence on the boundary condition, and can turn it from slippery to sticky. It is therefore essential to integrate the control of menisci in fluidic microsystems designed to reduce wall friction.

Here, we investigate slippage on superhydrophobic surfaces embedded with a square lattice of calibrated cylindrical holes (see Fig. 1). The microstructure is made by photolithography and electrochemical etching[13]. The plain surfaces are hydrophilic, and wetted by water in the so-called 'Wenzel' regime, that is, with the liquid filling the holes. Silanized surfaces are superhydrophobic, and the favoured wetting regime of water is the Cassie regime (advancing contact angle 155°, hysteresis of 9°), with microbubbles trapped in the cylindrical holes. The slippage on those surfaces is characterized by the effective slip length B, which corresponds to the distance between the top of the walls of the patterned surface and the virtual no-slip plane where the mean velocity profile extrapolates to zero. The higher the effective slip length, the higher the slippage and the smaller the interfacial friction.

We study the effective slippage on these surfaces with a dynamic surface force apparatus[14] (SFA). A newtonian liquid (a mixture of water and glycerol with similar wetting properties as water, with a viscosity $\eta = 39 \pm 2$ mPa s) is confined between the microstructured plane and a smooth non-slipping sphere of radius R. The dynamic SFA measures the complex force response $G(\omega) = F(\omega)/h_0$ acting on the surfaces when the sphere is oscillated in the normal direction with an amplitude h_0 and a frequency $\omega/2\pi$. It is measured for varying values of the mean distance D between the sphere apex and the top of the plane. The imaginary part of the complex force response $G''(\omega)$ is the viscous damping due to the flow and can be linked to the effective (averaged) hydrodynamic boundary condition on the plane. According to the theory[15], the far-field asymptote of the inverse of the viscous damping G''^{-1} with respect to the distance D intersects the D axis at the position of the virtual no-slip surface, directly giving the value of the effective slip length B as defined above. The slope of the asymptote is equal to $[6\pi\omega\eta R^2]^{-1}$. The real part $G'(\omega)$, for a newtonian liquid, is a signature of the elastic deformation of the surfaces.

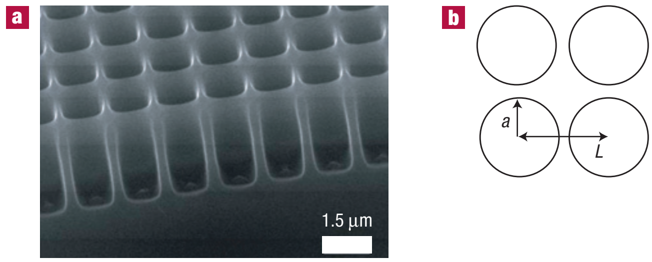

Figure 1 Microstructured surfaces. Description of the surfaces used. **a**, Scanning electron micrograph (taken under an angle) of the microstructured surfaces studied. **b**, The surfaces are modelled by smooth planes with holes of radius $a = 0.65 \pm 0.03$ μm and height $H = 3.5$ μm, laid on a square lattice of period $L = 1.4$ μm. The surface fraction of the solid ($\phi_S = 1 - (\pi a^2/L^2)$) is equal to 0.32 ± 0.06.

We compare two situations: the hydrophilic plane (Wenzel regime, no bubbles) which is the reference situation, and the superhydrophobic plane (Cassie regime, trapped bubbles). The radius of the sphere is $R = 3.25 \pm 0.05$ mm in the hydrophilic case and $R = 3.05 \pm 0.05$ mm in the superhydrophobic case. Both experiments are carried out at an excitation frequency of 19 Hz.

In the hydrophilic case, we show in Fig. 2a the inverse of the viscous damping as a function of the distance D between the surfaces. The linear extrapolation of the viscous damping intersects the D axis at a distance of 105 ± 10 nm from the origin, which corresponds to an effective slip length B of 105 ± 10 nm. In this reference situation, the extrapolated no-slip plane lies underneath the top of the wall, as expected, because some of the liquid inside the holes participates in the flow[16]. As shown in Fig. 2b, the real part G' of the force response is equal to zero, as there is no elastic deformation of the surface.

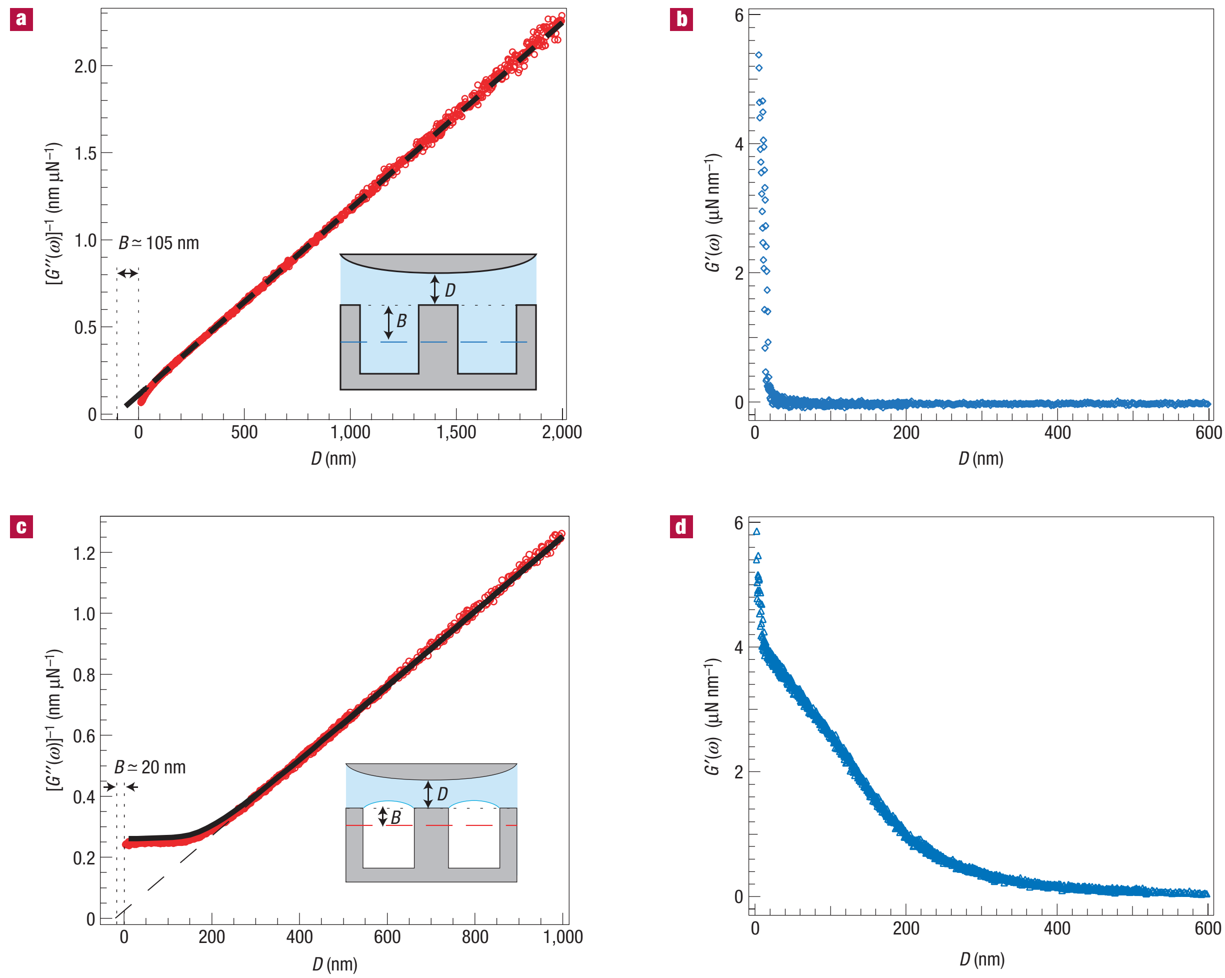

Figure 2 Nanorheology over microstructured surfaces. Flow between a Pyrex sphere and a textured microstructured plane (see insets). **a**,**b**, The surface is hydrophilic; the liquid fills the holes. **c**,**d**, The surface is superhydrophobic; the liquid does not fill the holes. **a** and **c** show the evolution of the inverse of the viscous damping G''^{-1} as a function of the distance D between the surfaces. The far-field asymptote (dashed line) allows the determination of the effective slip length B. **b** and **d** show the evolution of the elastic part G' as a function of the distance D; a value equal to zero corresponds to a rigid response (**b**). Solid line (**c**): Fitting results for a model based on the local elasticity of the superhydrophobic surface embedded with bubbles, with a surface stiffness $\kappa = 9.5 \times 10^{11}$ N m^{-3} and a slip length B of 20 nm.

In the superhydrophobic case (Fig. 2c), the asymptote of the inverse of the viscous damping G''^{-1} intersects the D axis at a distance $B = 20 \pm 10$ nm from the top of the walls, showing a much smaller effective slip length in the presence of microbubbles than in the hydrophilic case. In addition, at small distances the damping is quite different from that observed in the hydrophilic case. This saturation of the damping is an elastohydrodynamic effect, owing to the compression of the bubbles trapped inside the holes of the superhydrophobic surface. In Fig. 2d, the elastic part G' of the response function, which is not zero, shows directly the elastic contribution of the bubbles which deform under the pressure induced by the flow. This elastic response confirms the presence of gas trapped in the surface holes. The striking point of these results is to show a smaller effective slip length ($B = 20 \pm 10$ nm) in the presence of microbubbles, than without any gas phase trapped at the boundary ($B = 105 \pm 10$ nm). This demonstrates the fact that the presence of gas trapped at an interface does not always have a lubricating effect on the boundary flow.

We evaluate the stiffness of the microbubbles by comparing the force response to a continuous elastohydrodynamic model with a locally deformable surface: the surface displacement $\xi(r,t)$ at a distance r from the sphere-plane axis is assumed to depend linearly on the local liquid pressure $\xi(r,t) = \kappa^{-1} p(r,t)$. Fitting the experimental data with a numerical resolution of this model (solid line in Fig. 2c) confirms the effective slip length $B = 20 \pm 10$ nm on the plane, and yields a local surface stiffness $\kappa = (9.5 \pm 1.0) \times 10^{11}$ N m^{-3}. From this value, the stiffness K_{bubble} of a single bubble can be determined: $K_{\text{bubble}} = \mathrm{d}P_{\text{liquid}}/\mathrm{d}V_{\text{bubble}} = \kappa/L^2$, where P_{liquid} is the mean pressure of the liquid above the bubble of volume V_{bubble} and L is the lattice periodicity. The stiffness is dominated by the stiffness of the meniscus $K_{\text{cap}} = 2\gamma\cos\theta(1+\cos\theta)^2/\pi a^4$, where θ is the protrusion angle of the meniscus (defined in the inset of Fig. 3). Taking into account the error bars in the determination of the hole radius from scanning electron micrographs ($a = 0.65 \pm 0.03$ µm) and in the water/glycerol surface tension ($\gamma = 63 \pm 3$ mN m^{-1}), we can estimate the angle of the protruding menisci: $30° < \theta < 60°$. This corresponds to a height of the microbubbles of about 200–400 nm above the solid surface.

Is this protruding geometry of the menisci responsible for the low slip length measured? To answer this question, we study numerically the influence of the meniscus shape on the hydrodynamic boundary condition, with a three-dimensional finite-element method (Comsol). We solve for a Couette flow between a smooth surface moving at a velocity U_0 and a fixed model surface made of a square lattice of cylindrical holes with the same parameters as the experiment (see Fig. 1). To account for the experimental uncertainty on the hole radius, we consider three values for the radius ($a = 0.62$, 0.65 and 0.68 μm). We take a no-slip boundary condition on each solid–liquid interface.

We first consider our reference case: the Wenzel wetting regime with the liquid filling the holes. In this case, we get an effective slip length $B_{\text{filled}} = 55 \pm 10$ nm in relatively good agreement with the value measured experimentally in the hydrophilic case (105 ± 10 nm). The difference between those values comes from the experimental error (offset) in the distance D measured due to the wall roughness, a few tens of nanometres (the top of the roughness is the reference plane in SFA experiments).

In the Cassie regime, when bubbles fill the holes, we calculate the effective slip as a function of the shape of the meniscus characterized by the protrusion angle θ (Fig. 3). For this we consider simplified local boundary conditions on the free surface: the meniscus is anchored at the edge of the holes and its shape is a fixed spherical cap that does not depend on the stress. This approximation is valid in the limit of small capillary numbers, which is representative of our experiments in which the capillary number is always smaller than 10^{-4}. Angles θ smaller than $-30°$ are not considered because they would correspond to negative values of the pressure in the gas phase. For all other values of θ, the meniscus is stable (its compressibility is positive). In addition, we neglect the viscosity of the gas phase and assume a perfect slip boundary condition locally on the meniscus.

The numerical results (Fig. 3) clearly show the decrease in slip length due to the meniscus curvature. A huge decrease of the effective slip length is obtained for protruding menisci: for $\theta > 45°$, the slip lengths become smaller than in the Wenzel case, that is, without any gas phase trapped on the surface. At larger angle values, the effective slip lengths become negative, accounting for an immobilized layer of the liquid close to the wall. In this limit, the liquid–solid friction is higher than on a non-slipping flat solid surface without holes. Our experimental results lie in the region where the effective slip length decreases strongly with the menisci protrusion. The SFA value for the effective slip length, $B = 20 \pm 10$ nm, plotted as a function of the experimental determination of the protrusion angle, $30° < \theta < 60°$ (orange rectangle), is in quantitative agreement with the numerical results. Thus, the 'sticky' behaviour observed experimentally is actually explained by the effect of the menisci curvature.

This experiment shows quantitatively that the boundary condition of a liquid flowing on a composite surface embedded with microbubbles depends dramatically on the shape of the gas–liquid interfaces. Contrary to what is often believed, the presence of gas at the solid–liquid interface does not always reduce the friction. A gas phase can also promote high friction, by trapping an immobile liquid layer of significant thickness above the solid wall. Our result is the first experimental evidence of Richardson's and Jansons' predictions[17,18], which showed that a perfectly slippery surface can provide a no-slip boundary condition if it is rough enough. In view of this result, it is not clear that the slip lengths of micrometric size reported in the literature on smooth hydrophobic surfaces can actually be explained by the presence of nanobubbles. Indeed, as described in ref. 19, the nanobubbles that exist on hydrophobic surfaces are not flat; they resemble spherical caps with heights of the order of 10 nm and diameters of the order of 100 nm, an aspect ratio close to that of our bubbles (1.3 μm in diameter and about 250 nm in height). More specifically, the stable nanobubbles demonstrated in ref. 19 are only 4 to 20 times smaller than ours (60–300 nm in diameter), so that we would expect our macroscopic analysis to hold. Finally, our result also shows that controlling slippage at the wall using superhydrophobic surfaces in microfluidics applications is still an open problem for surface engineering. Geometry is a key element and patterns should be designed to minimize the meniscus curvature. With contiguous grooves for instance, or with posts—for which the gas phase is connected to a reservoir—the shape of the meniscus is expected to be less pronounced and the negative impact on the slippage should be smaller. Conversely, controlling the shape of the meniscus would provide a means of fine tuning the boundary condition at the wall.

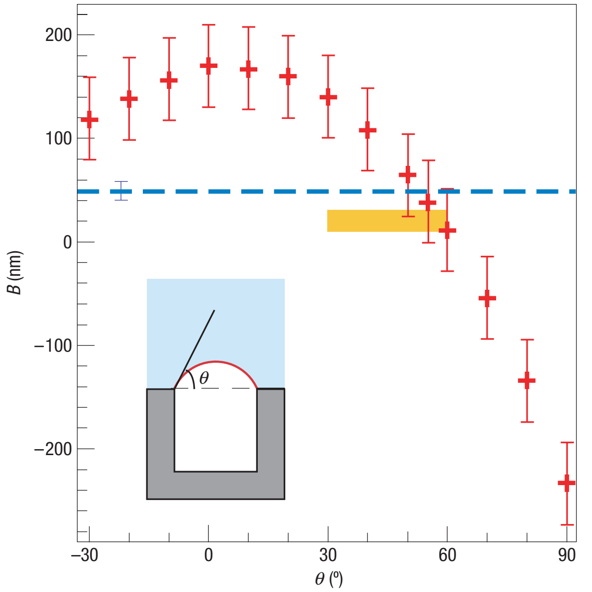

Figure 3 Evolution of the slip length with the meniscus shape. Red crosses: Numerical values for an angle θ of the meniscus. Dashed blue line: Numerical value in the hydrophilic case when the liquid fills the holes. The width of the error bars corresponds to the numerical values obtained for the radius a, $0.62 \leq a \leq 0.68$ μm. Orange rectangle: SFA experimental value (taking into account the error bars). Inset: Schematic diagram of the protrusion angle θ formed by the meniscus in the superhydrophobic case.

METHODS

The numerical calculation of the effective slip length on the patterned surfaces is made with the three-dimensional finite-element method Comsol solving for a Couette flow in a unit cell of the square lattice. The bottom surface is a square of size $L \times L$ ($L = 1.4$ μm) with a cylindrical hole of depth $H = 3.5$ μm and radius $a = 0.62$, 0.65 or 0.68 μm in its middle (this corresponds to the experimental determination of the pattern parameters). The upper surface is a flat plane located at a distance $z = d$ of the top of the bottom surface. This unit cell is filled with a newtonian liquid of viscosity η. The Couette flow is produced by keeping fixed the lower surface and by moving the upper one at a velocity U_0 in the x direction, parallel to a horizontal axis of the unit cell. The velocity profile is assumed periodic in the x direction, and the velocity in the $y = 0$ and $y = L$ planes has no component on the y axis. A no-slip boundary condition is assumed on all liquid–solid surfaces. When calculating the flow on a bubble, a perfect slip boundary condition is assumed at the liquid–gas interface. The effective slip length is derived from the viscous force F acting on the upper surface. The viscous force is obtained by integrating the x component of the tangential stress σ_{xz} $(z = d) = \eta \cdot \mathrm{d}v_x/\mathrm{d}z$. The slip length is then given by $B = (U_0 \eta L^2/F) - d$. It is checked that this value does not depend significantly on the distance d, which is varied between $d = 3a$ and $6a$.

In the calculation of the flow on a bubble, the liquid–gas meniscus is treated as a rigid boundary. We check separately for the stability of the meniscus by calculating analytically its compressibility (that is, the stiffness of the bubble). Neglecting the gas compressibility, which has a stabilizing effect, the stiffness of the meniscus K_{cap} is always positive, so the meniscus is stable over the whole range of values of θ we considered.

Received 23 May 2007; accepted 27 June 2007; published 22 July 2007.

References

1. Vinogradova, O. L. *et al*. Submicrocavity structure of water between hydrophobic and hydrophilic walls as revealed by optical cavitation. *J. Colloid Interface Sci.* **173**, 443–447 (1995).
2. de Gennes, P. G. On fluid/wall slippage. *Langmuir* **18**, 3413–3414 (2002).
3. Cottin-Bizonne, C., Barrat, J.-L., Bocquet, L. & Charlaix, E. Low-friction flows of liquid at nanopatterned interfaces. *Nature Mater.* **2**, 237–240 (2003).
4. Tretheway, D. C. & Meinhart, C. D. A generating mechanism for apparent fluid slip in hydrophobic microchannels. *Phys. Fluids* **16**, 1509–1515 (2004).
5. Quere, D. Non sticking drops. *Rep. Prog. Phys.* **68**, 2495–2532 (2005).
6. Philip, J. R. Integral properties of flows satisfying mixed no-slip and no-shear conditions. *Z. Angew. Math. Phys.* **23**, 960–968 (1972).
7. Lauga, E. & Stone, H. A. Effective slip in pressure-driven Stokes flow. *J. Fluid Mech.* **489**, 55–77 (2003).
8. Cottin-Bizonne, C., Barentin, C., Charlaix, E., Bocquet, L. & Barrat, J.-L. Dynamics of simple liquids at heterogeneous surfaces: Molecular-dynamics simulations and hydrodynamic description. *Eur. Phys. J. E* **15**, 427–438 (2004).
9. Sbragaglia, M. & Prosperetti, A. Effective velocity boundary condition at a mixed slip surface. *J. Fluid Mech.* **578**, 435–451 (2007).
10. Joseph, P. *et al*. Slippage of water past superhydrophobic carbon nanotube forests in microchannels. *Phys. Rev. Lett.* **97**, 156104 (2006).
11. Ou, J., Perot, B. & Rothstein, J. P. Laminar drag reduction in microchannels using ultrahydrophobic surfaces. *Phys. Fluids* **16**, 4635–4643 (2004).
12. Ou, J. & Rothstein, J. P. Direct velocity measurements of the flow past drag-reducing ultrahydrophobic surfaces. *Phys. Fluids* **16**, 103606 (2005).
13. Kleimann, P., Badel, X. & Linnros, J. Toward the formation of three-dimensional nanostructures by electrochemical etching of silicon. *Appl. Phys. Lett.* **86**, 183108 (2005).
14. Restagno, F., Crassous, J., Charlaix, E., Cottin-Bizonne, C. & Monchanin, M. A new surface forces apparatus for nanorheology. *Rev. Sci. Instrum.* **73**, 2292–2297 (2002).
15. Vinogradova, O. I. Drainage of a thin liquid-film confined between hydrophobic surfaces. *Langmuir* **11**, 2213–2220 (1995).
16. Tachie, M. F., James, D. F. & Currie, I. G. Slow flow through a brush. *Phys. Fluids* **16**, 445–451 (2004).
17. Richardson, S. No-slip boundary condition. *J. Fluid Mech.* **59**, 707–719 (1973).
18. Jansons, K. M. Determination of the macroscopic (partial) slip boundary condition for a viscous flow over a randomly rough surface with a perfect slip microscopic boundary condition. *Phys. Fluids* **31**, 15–17 (1988).
19. Borkent, B. M., Dammer, S. M., Schönherr, H., Vancso, G. J. & Lohse, D. Superstability of surface nanobubbles. *Phys. Rev. Lett.* **98**, 204502 (2007).

Acknowledgements

We would like to thank L. Bocquet, P.-Y. Verilhac and X. Badel. We acknowledge support from ANR pNANO.
Correspondence and requests for materials should be addressed to C.C.-B.

Competing financial interests

The authors declare no competing financial interests.

Reprints and permission information is available online at http://npg.nature.com/reprintsandpermissions/